Solvation of Copper Ions by Acetone. Structures and Sequential Binding Energies of $Cu^+(acetone)_x$, $x = 1–4$ from Collision-Induced Dissociation and Theoretical Studies

Y. Chu, Z. Yang, and M. T. Rodgers
Department of Chemistry, Wayne State University, Detroit, Michigan

Collision-induced dissociation of $Cu^+(acetone)_x$, $x = 1–4$, with Xe is studied as a function of kinetic energy using guided ion beam mass spectrometry. In all cases, the primary and lowest energy dissociation channel observed is endothermic loss of one acetone molecule. The primary cross section thresholds are interpreted to yield 0 and 298 K bond energies after accounting for the effects of multiple ion-neutral collisions, internal energy of the complexes, and dissociation lifetimes. Density functional calculations at the B3LYP/6-31G* level of theory are used to determine the structures of these complexes and provide molecular constants necessary for the thermodynamic analysis of the experimental data. Theoretical bond dissociation energies are determined from single point calculations at the B3LYP/6-311+G(2d,2p) and MP2(full)/6-311+G(2d,2p) levels, using the B3LYP/6-31G* optimized geometries. The experimental bond energies determined here are in good agreement with previous experimental measurements made in a high-pressure mass spectrometer for the sum of the first and second bond energy (i.e., $Cu^+(acetone)_2 \rightarrow Cu^+ + 2$ acetone) when these results are properly anchored. The agreement between theory and experiment is reasonable in all cases, but varies both with the size of the cluster and the level of theory employed. B3LYP does an excellent job for the $x = 1$ and 3 clusters, but is systematically low for the $x = 2$ and 4 clusters such that the overall trends in sequential binding energies are not parallel. In contrast, all MP2 values are somewhat low, but the overall trends parallel the measured values for all clusters. The trends in the measured $Cu^+(acetone)_x$ binding energies are explained in terms of 4s-3d σ hybridization effects and ligand-ligand repulsion in the clusters. (J Am Soc Mass Spectrom 2002, 13, 453–468) © 2002 American Society for Mass Spectrometry

Recently there has been growing interest in the development of ligands that are able to effectively and selectively bind metal ions through multiple noncovalent interactions. Potential uses for such ligands include various applications, e.g., sensing elements in cation selective electrodes, the removal of metals from environmental sources and toxic waste stores, and for use in biological transport mechanisms for drug delivery schemes. This interest has led to a great deal of research involving the synthesis of such ligands, the measurement of binding constants in solution of such ligands in aqueous and a variety of organic solvents, and gas phase studies of the binding affinities of such ligands to various metal ions. One advantage of the gas phase studies is that they allow the direct determination of the strength of the intrinsic interactions between the metal ion and the ligand in the absence of solvents effects. However, the binding in solution can differ markedly from that observed in the gas phase as a result of the influence of solvent on these interactions. In general, the solvent significantly weakens electrostatic forces (and hydrogen bonding interactions when present) between ions and ligands by shielding and competing for their attractions. The relative behavior in solution often parallels that of the gas phase, but in some cases a marked change in the relative binding affinities is observed. A number of examples of solvent-induced selectivity have been documented including the interaction of alkali metal ions with benzene [1–3], 18-crown-6 [4–8], and dibenzo-18-crown-6 [4, 9]. By measuring the strength of noncovalent interactions both in solution and the gas phase, the influence of the solvent on such interactions can in

Published online March 26, 2002

In honor of P. B. Armentrout in celebration of his winning the 2001 Biemann Medal, in thanks for his numerous contributions to ion thermochemistry, and in appreciation for his mentoring and friendship.

Address reprint requests to Dr. M. T. Rodgers, Department of Chemistry, Wayne State University, Detroit, MI 48202. E-mail: mrodgers@chem.wayne.edu

1044-0305/02/$20.00
PII S1044-0305(02)00355-0

Received December 17, 2001
Revised January 16, 2002
Accepted January 16, 2002

principle be elucidated. Alternatively, insight into the influence of solvent on noncovalent interactions between an ion and a ligand can also be gained by considering the competition between the solvation of the ion, and complexation of the ion by the ligand of interest, reaction 1.

$$M^+(\text{Solvent})_x + \text{Ligand} \rightarrow M^+(\text{Ligand}) + x\ \text{Solvent} \quad (1)$$

Such analyses proved useful in understanding the role of solvent in determining the binding preferences of benzene [1] and 18-crown-6 in aqueous solution [5–8]. This seminal work suggests that accurate gas phase measurements of binding energies between metal ions and various ligands combined with analogous measurements of solvation enthalpies can be used to provide a detailed understanding of such interactions in solution. A particularly important aspect of such gas-phase studies is that the measurement of solvation enthalpies of metal ions can be potentially useful in the study of a wide variety of ligands. This provides motivation for the work performed here as well as a series of related studies currently being performed in our laboratory in which the solvation enthalpies of a variety of metal ions are being examined to commonly used solvents [10, 11]. In particular, we are interested in extending such microsolvation studies to include metal ions other than the alkalis, and solvents other than water. There are two major reasons for this extension. First, solvent induced selectivity is dependent upon the solvent. For example, the observed selectivity for binding of alkali metal ions by dibenzo-18-crown-6 in acetonitrile, an aprotic solvent, differs from the selectivity observed in protic solvents, such as water and methanol [9]. Second is our interest in thiacrown ethers, which preferentially bind transition metal ions over alkali metal ions.

Much of our recent work has made use of quantitative threshold collision-induced dissociation (CID) methods to obtain accurate thermodynamic information on a variety of noncovalently bound metal–ligand complexes. These studies have either directly probed the interaction between metal ions and organic [12–17] and biological ligands [18, 19], or have examined solvation of metal ions by various solvents [10, 11, 20, 21]. In the present study, we use guided ion beam mass spectrometry to collisionally excite $Cu^+(\text{acetone})_x$ clusters. The kinetic energy-dependent cross sections for the CID processes are analyzed using methods developed previously [22]. The analysis explicitly includes the effects of the internal and translational energy distributions of the reactants, multiple collisions, and the lifetime for dissociation. We derive $(\text{acetone})_{x-1}Cu^+$–acetone bond dissociation energies (BDEs) for all of the complexes, $x = 1–4$, and compare these results to ab initio and density functional calculations performed here. Comparison is also made to previous experimental measurements for the total binding energy of the $Cu^+(\text{acetone})_2$ complex [23, 24]. Finally, the trends in the sequential binding energies of Cu^+ to acetone measured here are compared to a variety of other ligands previously examined including: CH_3CN [11], H_2O [25, 26], NH_3 [27], and CH_3OCH_3 [28].

Experimental

General Procedures

Cross sections for collision-induced dissociation of $Cu^+(\text{acetone})_x$ clusters are measured using a guided ion beam tandem mass spectrometer that has been described in detail previously [15]. The $Cu^+(\text{acetone})_x$ clusters are generated in a flow tube ion source by condensation of the copper ion and neutral acetone molecule(s). These complexes are collisionally stabilized and thermalized by $\sim 10^5$ collisions with the He and Ar bath gases such that ions emanating from the source region are well described by a Maxwell-Boltzmann distribution at room temperature. The ions are extracted from the source, accelerated, and focused into a magnetic sector momentum analyzer for mass analysis. Mass-selected ions are decelerated to a desired kinetic energy and focused into an octopole ion guide, which traps the ions in the radial direction [29]. A static gas cell containing the neutral collision gas, Xe, surrounds the octopole. In general, Xe is employed for all of our CID measurements and is used here because it is heavy and polarizable and therefore leads to more efficient kinetic to internal energy transfer in the CID process [30–32]. To ensure that multiple ion-neutral collisions are improbable, the pressure of Xe in the cell is kept low, and varied between 0.05 and 0.20 mTorr for different experiments. Product and unreacted beam ions drift to the end of the octopole where they are focused into a quadrupole mass filter for mass analysis and subsequently detected with a secondary electron scintillation detector and standard pulse counting techniques.

Ion intensities are converted to absolute cross sections as described previously [33]. Absolute uncertainties in cross section magnitudes are estimated to be ±20 %, which are largely the result of errors in the pressure measurement and the length of the interaction region. Relative uncertainties are approximately ±5%.

Ion kinetic energies in the laboratory frame, E_{lab}, are converted to energies in the center of mass frame, E_{CM}, using the formula $E_{CM} = E_{lab}\, m/(m + M)$, where M and m are the masses of the ionic and neutral reactants, respectively. All energies reported below are in the CM frame unless otherwise noted. The absolute zero and distribution of the ion kinetic energies are determined using the octopole ion guide as a retarding potential analyzer as previously described [33]. The distribution of ion kinetic energies is nearly Gaussian with a fwhm typically between 0.2 and 0.4 eV (lab) for these experi-

Table 1. Vibrational frequencies and average vibrational energies at 298 K

Species	E_{vib}, eV[a]	Vibrational frequencies, cm^{-1} [b]
acetone	0.11 (0.01)	36, 132, 368, 477, 521, 771, 877, 880, 1074, 1109, 1221, 1383, 1385, 1461, 1465, 1469, 1486, 1788, 2985, 2992, 3040, 3047, 3104, 3105
Cu^+(acetone)	0.14 (0.01)	84, 127, 308, 486, 489, 506, 848, 873, 904, 1101, 1105, 1263, 1391, 1393, 1440, 1447, 1461, 1468, 1700, 2992, 3001, 3046, 3054, 3116, 3117
Cu^+(acetone)$_2$	0.32 (0.02)	29, 30 (2), 96, 98, 155, 156, 235, 328, 452, 485 (2), 497 (2), 515, 833, 837, 878, 880, 904 (2), 1098, 1100, 1102 (2), 1261 (2), 1393 (2), 1396 (2), 1445, 1446, 1450 (2), 1463 (2), 1472 (2), 1714, 1724, 2993 (2), 3000, 3001, 3047 (2), 3055 (2), 3114 (3), 3115
Cu^+(acetone)$_3$	0.48 (0.03)	**23**, **26**, **30**, **33**, **36**, 38, 53, 75, 77, 87, 98, 111, 128, 135, 143, 160, 171, 226, 260, 281, 392, 401, 413, 477, 480, 481, 525, 568, 576, 802, 806, 807, 886, 887, 888, 904, 911, 913, 1076, 1077, 1084, 1100, 1103, 1106, 1253, 1261, 1262, 1389, 1390, 1393, 1397, 1398 (2), 1450, 1451, 1452, 1453, 1455 (2), 1460, 1462, 1466, 1474, 1476, 1478, 1681, 1683, 1704, 2989, 2990, 2991, 2996 (2), 2998, 3048 (2), 3049, 3055, 3057 (2), 3087, 3091, 3101, 3113, 3115, 3117
Cu^+(acetone)$_4$	0.66 (0.04)	**5**, **14**, **21** (**2**), **25**, **31**, **34**, 35, 44, 52, 61, 73, 79, 85, 87, 95, 103, 109, 116, 122, 133, 139, 148, 156, 188, 221, 241, 242, 387, 392, 394, 395, 474, 476, 477, 479, 543, 545, 549, 556, 793, 794 (2), 798, 882, 883, 884, 885, 905, 917, 918, 922, 1071, 1073, 1075, 1081, 1100, 1102, 1103, 1104, 1250, 1251 (2), 1252, 1389, 1390, 1391 (2), 1395 (3), 1397, 1452 (2), 1453, 1454, 1455, 1456, 1458 (2), 1463 (2), 1466, 1467, 1475, 1476, 1480, 1485, 1683, 1689, 1690, 1699, 2987, 2988, 2992 (3), 2993, 2998, 2999, 3047 (4), 3056, 3058, 3060, 3062, 3097, 3101, 3110 (3), 3112, 3113, 3115

[a]Uncertainties listed in parentheses are determined as described in the text.
[b]Vibrational frequencies (scaled by 0.9804) are obtained from a vibrational analysis of the geometry optimized structures for these species obtained from density functional calculations performed at the B3LYP/6-31G* level. Frequencies indicated in boldface correspond to non-imaginary CH_3 torsional motions and were replaced by 1-D rotors as indicated in Table 2.

ments. The uncertainty in the absolute energy scale is ±0.05 eV (lab).

Even when the pressure of the reactant neutral is low, it has previously been demonstrated that the effects of multiple collisions can significantly influence the shape of CID cross sections [26]. Therefore, we have performed pressure-dependent studies of all cross sections examined here. Data free from pressure effects are obtained by extrapolating to zero reactant pressure, as described previously [26]. Thus, outcomes reported below result from single bimolecular encounters.

Thermochemical Analysis

The threshold regions of the reaction cross sections are modeled using eq 2,

$$\sigma(E) = \sigma_0 \sum_i g_i(E + E_i - E_0)^n/E \quad (2)$$

where σ_0 is an energy independent scaling factor, E is the relative translational energy of the reactants, E_0 is the threshold for reaction of the ground electronic and ro-vibrational state, and n is an adjustable parameter that describes the efficiency of kinetic to internal energy transfer [34]. The summation is over the ro-vibrational states of the reactant cluster ions, i, where E_i is the excitation energy of each state and g_i is the population of those states ($\Sigma g_i = 1$). The populations of excited ro-vibrational levels are not negligible even at 298 K as a result of the many low-frequency modes present in these ions. The relative reactivity of all ro-vibrational states, as reflected by σ_0 and n, is assumed to be equivalent.

The Beyer-Swinehart algorithm [35] is used to determine the density of the ro-vibrational states, and the relative populations, g_i are calculated by an appropriate Maxwell-Boltzmann distribution at 298 K, the temperature appropriate for the reactants. The vibrational frequencies and rotational constants are derived from electronic structure calculations as described in the Theoretical Calculations section. The average vibrational energies at 298 K of the Cu^+(acetone)$_x$ clusters are given in Table 1. We have increased and decreased the scaled vibrational frequencies by 10 % to encompass the range of average scaling factors needed to bring the calculated frequencies into agreement with experimentally determined frequencies as found by Pople et al. [36]. The corresponding change in the average vibrational energy is taken to be an estimate of one standard deviation of the uncertainty in vibrational energy (Table 1).

We also consider the possibility that collisionally-activated cluster ions do not dissociate on the time scale of our experiment (approximately 10^{-4} s) by including statistical theories for unimolecular dissociation, specifically Rice-Ramsperger-Kassel-Marcus (RRKM) theory, into eq 2 as described in detail elsewhere [22, 37]. This requires sets of ro-vibrational frequencies appropriate for the energized molecules and the transition states (TSs) leading to dissociation. The former sets are given in Tables 1 and 2, whereas we assume that the TSs are loose and product-like because the interaction between the copper ion and the acetone molecules is largely electrostatic. In this case, the TS vibrations used are the

Table 2. Rotational constants of $Cu^+(acetone)_x$, x = 1–4 in cm^{-1}

	Energized molecule		Transition state				
Reactant	1-D[a]	1-D[b]	2-D[c]	1-D[d]	1-D[b]	2D[d]	2-D[c,e]
$Cu^+(acetone)$	0.28	5.28 (2)	0.047	0.16	-	0.31	0.0048
$Cu^+(acetone)_2$	0.14	5.28 (4)	0.013	0.16, 0.28	5.28 (2)	0.31, 0.047	0.0064
$Cu^+(acetone)_3$	0.0097	5.28 (6)	0.016	0.16, 0.14	5.28 (4)	0.31, 0.013	0.0016
$Cu^+(acetone)_4$	0.011	5.28 (8)	0.0084	0.16, 0.0097	5.28 (6)	0.31, 0.016	0.0017

[a]Active external.
[b]1-D rotor replacing the frequency associated with CH_3 torsional motion (in many instances, the calculated frequency is imaginary). Degeneracies are given in parentheses.
[c]Inactive external.
[d]Rotational constants of the transition state treated as free internal rotors.
[e]Two-dimensional rotational constant of the transition state at the threshold energy for dissociation, treated variationally and statistically.

frequencies corresponding to the products, which are also found in Table 1. The transitional frequencies, those that become rotations and translations of the completely dissociated products, are treated as rotors, a treatment that corresponds to a phase space limit (PSL) and is described in detail elsewhere [22]. Two of the rotors are simply the two rotational constants of the acetone product with axes that are perpendicular to the reaction coordinate, and correspond to the its 2D rotational constant (0.31 cm^{-1}). In the Cu^+(acetone) system, which yields one atomic product, these are the only two transitional modes. For the larger clusters, three additional transitional modes exist. Two of these rotors are the rotational constants of the $Cu^+(acetone)_{x-1}$ product, again those that are perpendicular to the reaction coordinate. Of the two rotational constants of the products with axes that lie along the reaction coordinate, one is a transitional mode and is assigned as the remaining rotational constant of the acetone product (5.28 cm^{-1}). The other becomes the 1-D external rotor of the TS. These are listed in Table 2. The external rotations of the energized molecule and TS are also included in the modeling of the CID data. The 2D external rotational constant of the TS is determined by assuming that the TS occurs at the centrifugal barrier for the interaction of $Cu^+(acetone)_{x-1}$ with the neutral acetone molecule, calculated variationally as outlined elsewhere [22]. The 2-D external rotations are treated adiabatically but with centrifugal effects included. The adiabatic 2-D rotational energy is treated using a statistical distribution with explicit summation over the possible values of the rotational quantum number, as described in detail elsewhere [22].

The model represented by eq 2 is expected to be appropriate for translationally-driven reactions [38] and has been found to reproduce CID cross sections well [10, 11, 25, 30, 37, 39, 40]. The model is convoluted with the kinetic energy distributions of both the reactant cluster ion and neutral Xe atom, and a nonlinear least-squares analysis of the data is performed to give optimized values for the parameters σ_0, E_0, and n. The error associated with the measurement of E_0 is estimated from the range of threshold values determined for different zero-pressure extrapolated data sets, variations associated with uncertainties in the vibrational frequencies, and the error in the absolute energy scale, 0.05 eV (lab). For analyses that include the RRKM lifetime effect, the uncertainties in the reported E_0 values also include the effects of increasing and decreasing the time assumed available for dissociation by a factor of 2.

Equation 2 explicitly includes the internal energy of the ion, E_i. All energy available is treated statistically because the ro-vibrational energy of the reactants is redistributed throughout the ion upon impact with the collision gas. The threshold for dissociation is by definition the minimum energy required leading to dissociation and thus corresponds to formation of products with no internal excitation. The threshold energies for dissociation reactions determined by analysis with eq 2 are converted to 0 K bond energies by assuming that E_0 represents the energy difference between reactants and products at 0 K [41]. This assumption requires that there are no activation barriers in excess of the endothermicity of dissociation, which should be valid for the simple electrostatic bond fission reactions examined here [42].

Theoretical Calculations

To obtain model structures, vibrational frequencies, rotational constants, and energetics for the neutral acetone ligand and for the $Cu^+(acetone)_x$ clusters, density functional calculations were performed using Gaussian 98 [43]. Geometry optimizations and frequency analyses of the geometry optimized structures were performed at the B3LYP/6-31G* level [44, 45], When used to model the data or to calculate thermal energy corrections, the B3LYP/6-31G* vibrational frequencies are scaled by a factor of 0.9804 [46]. The scaled vibrational frequencies thus obtained for these systems are listed in Table 1, whereas Table 2 lists the rotational constants. Single point energy calculations were performed at the B3LYP/6-311+G(2d,2p) and MP2(full)/6-311+G(2d,2p) levels using the B3LYP/6-31G* optimized geometries. To obtain accurate bond dissociation energies, zero point energy (ZPE) corrections were applied and basis set superposition errors (BSSE) were subtracted from the computed dissociation energies in

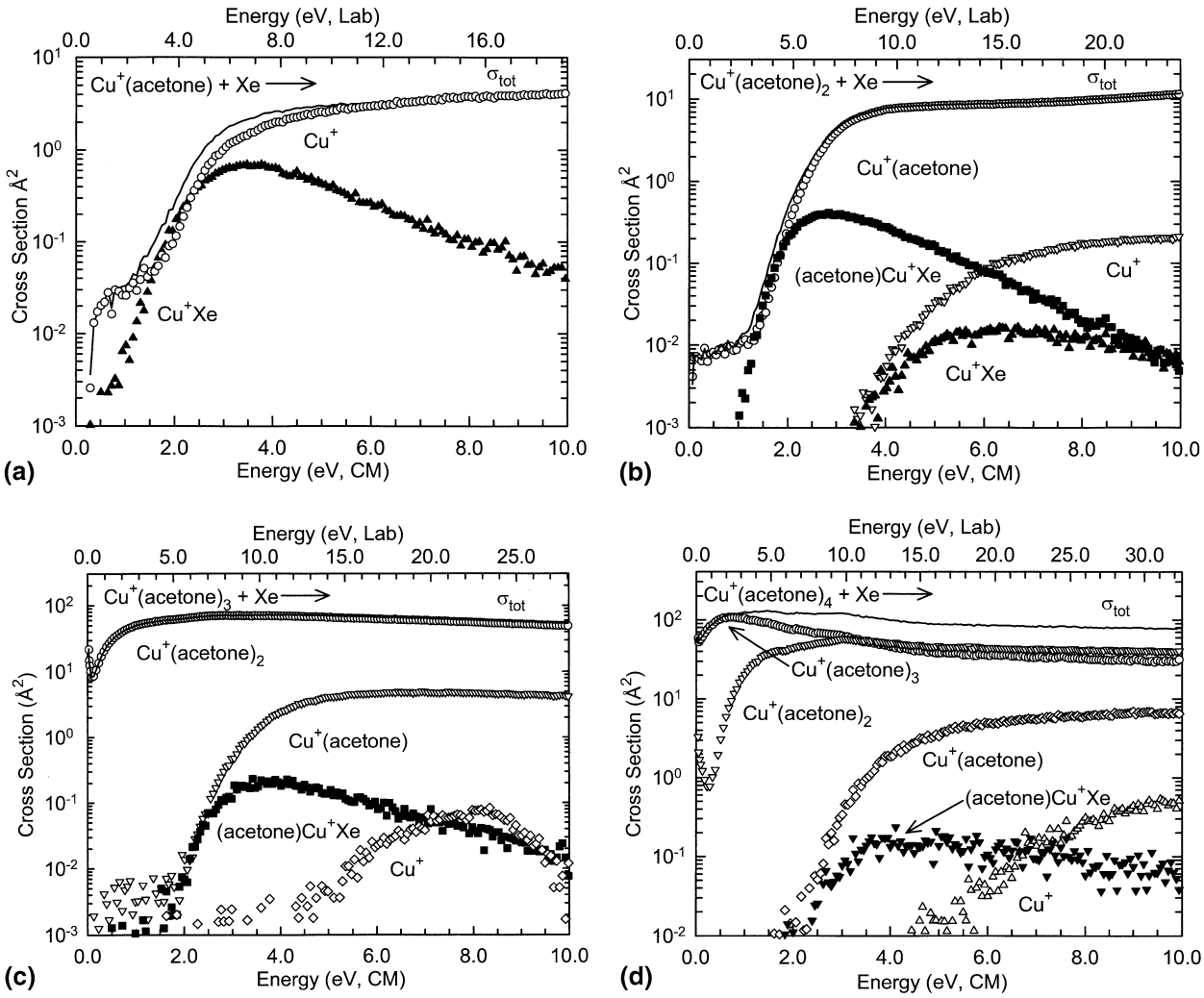

Figure 1. Cross sections for the collision-induced dissociation of the $Cu^+(acetone)_x$, $x = 1–4$ [parts (**a**) through (**d**), respectively], with Xe as a function of the kinetic energy in the center-of-mass frame (lower x-axis) and laboratory frame (upper x-axis). Data are shown for a Xe pressure of ~0.2 mTorr. Primary, secondary, tertiary, and quaternary product cross sections are shown as an open circle, open inverted triangle, open diamond, and open triangle, respectively. Primary, secondary, and tertiary ligand exchange product cross sections are shown as a filled triangle, filled square, and filled inverted triangle, respectively.

the full counterpoise approximation [47, 48]. The ZPE corrections are small, and are 3.3, 4.0, 4.4, and 1.9 kJ/mol for the $Cu^+(acetone)_x$, $x = 1–4$ clusters, respectively. Similarly, the BSSE corrections are small for the B3LYP calculations and range from 2.7 to 3.4 kJ/mol, but are significantly larger for the MP2 calculations, and range from 12.0 to 18.5 kJ/mol. As will be discussed later, the MP2 calculations may overestimate the BSSE corrections necessary.

Results

Cross Sections for Collision-Induced Dissociation

Experimental cross sections are shown in Figure 1 for the interaction of $Cu^+(acetone)_x$, $x = 1–4$, clusters with Xe. The sequential loss of intact acetone molecules and ligand exchange with Xe are the only processes observed in these systems over the collision energy range examined, typically 0 to 10 eV. The primary (most favorable) process for all clusters is the loss of a single acetone molecule in the CID reactions 3.

$$Cu^+(acetone)_x + Xe \rightarrow Cu^+(acetone)_{x-1} + acetone + Xe \quad (3)$$

The maximum cross section for reaction 3 (as well as the total cross section) increases in magnitude as the size of the $Cu^+(acetone)_x$ cluster increases, from ~3.8 to 11.6 to 72 to 108 Å^2 for $x = 1$ to 4, respectively. In contrast, the threshold for reaction 3 increases slightly from $x = 1$ to 2, and then decreases with increasing size of the cluster.

Table 3. Fitting parameters of eq 2, threshold dissociation energies at 0 K, kinetic shifts, and entropies of activation at 1000 K of $Cu^+(acetone)_x$, $x = 1–4$[a]

Species	σ_0[a]	n[b]	E_0[c] (eV)	E_0(PSL) (eV)	Kinetic shift (eV)	$\Delta S^{\ddagger}$(PSL) (J mol^{-1} K^{-1})
Cu^+(acetone)	3.0 (0.1)	1.2 (0.1)	2.21 (0.03)	2.06 (0.04)	0.15	30 (1)
$Cu^+(acetone)_2$	18.5 (0.9)	0.9 (0.1)	2.83 (0.04)	2.17 (0.07)	0.66	54 (3)
$Cu^+(acetone)_3$	61.2 (1.2)	1.2 (0.1)	0.72 (0.04)	0.67 (0.03)	0.05	113 (3)
$Cu^+(acetone)_4$	139.9 (7.1)[d]	0.7 (0.1)[d]	0.87 (0.04)[d]	0.63 (0.03)[d]	0.24[d]	82 (3)[d]
	129.6 (4.7)[e]	0.4 (0.1)[e]	0.95 (0.03)[e]	0.72 (0.03)[e]	0.23[e]	82 (3)[e]

[a]Uncertainties are listed in parentheses.
[b]Average values for loose PSL transition state.
[c]No RRKM analysis.
[d]Average values obtained when fitting the total cross section.
[e]Average values obtained when fitting the channel corresponding to the loss of one acetone molecule.

This behavior is not consistent with conventional ideas of ligation of gas-phase ions; i.e., stepwise sequential bond energies decrease because of increasing electrostatic repulsion between the ligands, causing the distance between the cation and ligands to increase. However, this behavior has been observed for other transition metal ions binding to a number of different ligands and can be explained in terms of 4s-3d σ hybridization effects as discussed below [11, 25, 27, 28].

Dissociation of additional acetone ligands is observed for the larger clusters at elevated energies. The shapes of the CID product cross sections confirm that these clusters are formed sequentially from the larger clusters, i.e., the primary product, $Cu^+(acetone)_{x-1}$, decreases as the secondary product, $Cu^+(acetone)_{x-2}$, appears. Similar behavior is observed for the higher order dissociation processes. In all cases, complete dissociation of the reactant cluster ion to produce bare Cu^+ is observed. As the size of the cluster increases, higher order dissociation (secondary, tertiary, and quaternary) accounts for a greater percentage of the total cross section, approximately 2, 8, and 60 % for $x = 2$, 3, and 4, respectively, at the highest energies examined. In general, the cross section magnitude decreases from the primary to secondary to tertiary to quaternary dissociation product at all energies examined. However, a deviation from this behavior occurs for the $Cu^+(acetone)_4$ cluster, where the primary and secondary product cross sections are observed to cross at ~3.5 eV such that the magnitude of the secondary product, $Cu^+(acetone)_2$, is larger than that of the primary product, $Cu^+(acetone)_3$, at high energies. This is likely the result of 4s-3d σ hybridization effects that leads to very strong binding for the first two ligands as discussed below.

The cross sections for ligand exchange decrease as the size of the cluster increases. For the case of $x = 1$, the cross section for the ligand exchange process is substantial, having a maximum nearly 17 % as large as the CID process. The magnitude of the ligand exchange cross section for the $x = 2$ cluster is half as large as it is for the $x = 1$ cluster, but its contribution to the total cross section has dropped by nearly a factor of five, such that it accounts for less than 4 % of the total cross section. Similarly, the ligand exchange cross sections continue to decrease with increasing solvation such that for the $x = 3$ and 4 clusters, the ligand exchange processes account for less than 0.3 and 0.2 % of the total cross section.

Threshold Analysis

The model of eq 2 was used to analyze the thresholds for reactions 3 in all four $Cu^+(acetone)_x$ systems. As previously discussed [30, 37, 39], the analysis of the primary CID thresholds provides the most reliable thermochemistry for such studies. This is because secondary and higher order products are more sensitive to lifetime effects, and additional assumptions are needed to quantitatively include the multiple products formed. The results of these analyses are provided in Table 3.

Experimental cross sections and fits to the data using a loose PSL model are shown in Figure 2 for loss of a single acetone molecule in the interaction of $Cu^+(acetone)_x$, $x = 1–4$, clusters with Xe (reaction 3). In all cases, the experimental cross sections for reaction 3 are accurately reproduced using a loose PSL TS model [22]. Previous work has shown that this model provides the most accurate assessment of the kinetic shifts for CID processes for electrostatic ion-molecule complexes [10–22]. Good reproduction of the data is obtained over energy ranges exceeding 3.5 eV and cross section magnitudes of at least a factor of 100. For the $x = 3$ and 4 clusters, the cross sections are finite at the lowest energies we examine, and hence, the reproduction does not cover quite the same magnitude range.

Two values of E_0 are listed in Table 3 for each cluster: One for analyses that do not include the RRKM lifetime effects, and one where the lifetime analysis is included (a loose PSL TS model). The unimolecular dissociation rate and therefore the kinetic shifts observed for these systems depend both upon the threshold energy and the number of acetone molecules surrounding the copper ion. The total number of vibrations increases with the size of the cluster from 27 for Cu^+(acetone) to 117 for $Cu^+(acetone)_4$. Likewise, the number of heavy at-

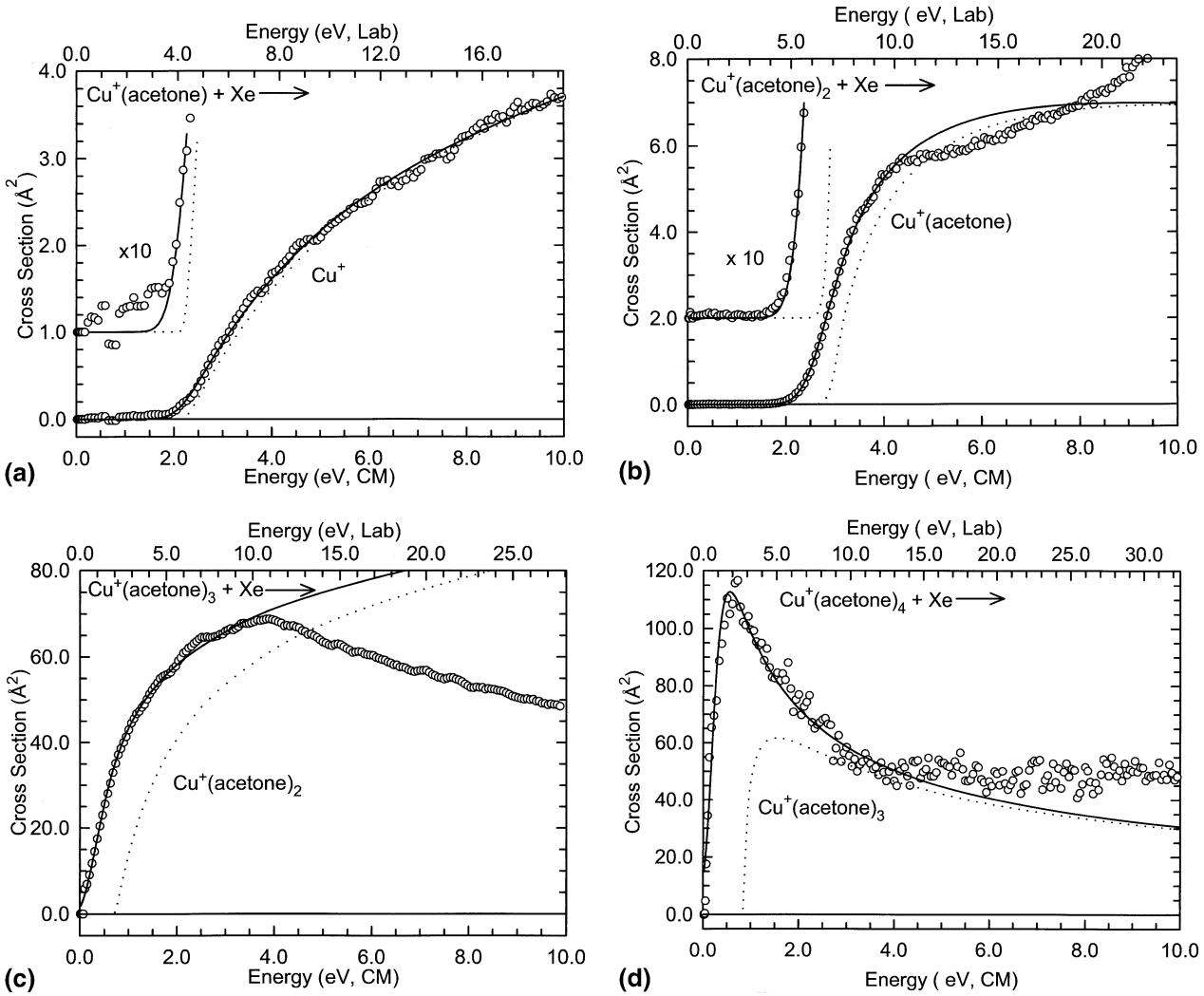

Figure 2. Zero-pressure-extrapolated primary product cross section for collision-induced dissociation of the $Cu^+(acetone)_x$, x = 1–4 [parts (**a**) through (**d**), respectively], with Xe in the threshold region as a function of kinetic energy in the center-of-mass frame (lower x-axis) and the laboratory frame (upper x-axis). A solid line shows the best fit to the data using eq 2 convoluted over the neutral and ion kinetic energy distributions. A dashed line shows the model cross sections in the absence of experimental kinetic energy broadening for reactants with an internal energy corresponding to 0 K.

oms increases from 5 to 17 as the size of the cluster increases from one to four acetone molecules. Thus the number of low frequency vibrations, those resulting in the largest impact on the density of states and therefore lifetime of the dissociating cluster, increase with the size of the cluster. The density of states also increases with energy such that kinetic shifts increase with threshold energy. Thus, dissociation of the Cu^+(acetone) system exhibits a modest kinetic shift of 0.15 eV. The $Cu^+(acetone)_2$ system exhibits a much larger kinetic shift of 0.66 eV, while $Cu^+(acetone)_3$ and $Cu^+(acetone)_4$ exhibit kinetic shifts of 0.05 and 0.24 eV, respectively. Thus, the kinetic shifts observed for the $Cu^+(acetone)_3$ and $Cu^+(acetone)_4$ clusters are smaller than for the $Cu^+(acetone)_2$ cluster as a result of the much weaker binding in the former systems (Table 3).

Two sets of fitting parameters are listed in Table 3 for the $Cu^+(acetone)_4$ cluster. These represent analysis of the total cross section for dissociation and an analysis of the cross section for loss of a single acetone molecule. The experimental cross section and fit to the total CID cross section using a loose PSL TS model is shown in Figure 3 for the interaction of the $Cu^+(acetone)_4$ cluster with Xe. For the x = 1, 2, and 3 clusters, these two models give identical results. For the x = 4 cluster, the fitting parameters obtained using the two models differ somewhat, and result in threshold values that differ by 0.09 eV. In this system, the cross section for reaction 3 is strongly affected by subsequent dissociation shortly after the threshold, such that the energy range unaffected by this second-order process is narrow. As a result, the fits of the total cross section were able to reproduce the data with higher fidelity.

The entropy of activation, ΔS^+, is a measure of the

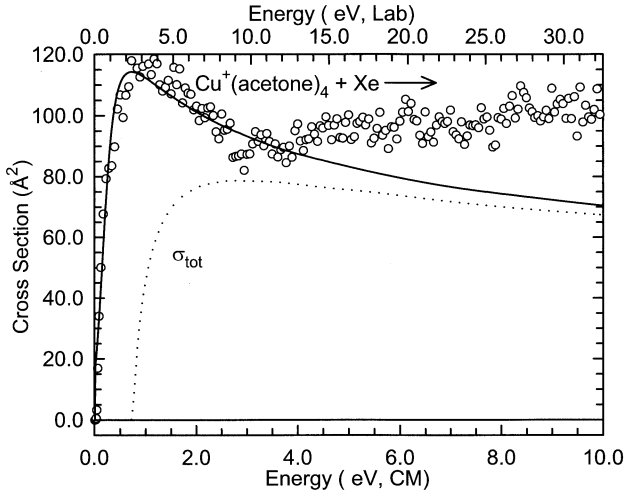

Figure 3. Zero-pressure-extrapolated total cross section for collision-induced dissociation of the $Cu^+(acetone)_4$ with Xe in the threshold region as a function of kinetic energy in the center-of-mass frame (lower x-axis) and the laboratory frame (upper x-axis). A solid line shows the best fit to the data using eq 2 convoluted over the neutral and ion kinetic energy distributions. A dashed line shows the model cross sections in the absence of experimental kinetic energy broadening for reactants with an internal energy corresponding to 0 K.

looseness of the TS and also a reflection of the complexity of the system. It is largely determined by the molecular parameters used to model the energized molecule and the TS, but also depends upon the threshold energy. Listed in Table 3, $\Delta S^{\ddagger}$(PSL) values at 1000 K range between 30 and 113 J K^{-1} mol^{-1} for the clusters containing one to four acetone molecules. The entropies of activation for the $x = 1$ and 2 clusters compare favorably to a wide variety of noncovalently bound complexes previously measured in our laboratory. These values also compare favorably to the $\Delta S^{\ddagger}_{1000}$ values in the range of 29–46 J K^{-1} mol^{-1} collected by Lifshitz for several simple bond cleavage dissociations of ions [49]. The much larger entropies of activation determined for the $x = 3$ and 4 clusters are likely the result of the conformational changes in the acetone ligands associated with steric crowding in these clusters.

Theoretical Results

Theoretical structures for the neutral acetone ligand and for the $Cu^+(acetone)_x$, $x = 1–4$ clusters were calculated as described above. Table 4 gives details of the final geometries for each of these species at the B3LYP/6-31G* level of theory. Results for the most stable conformation of the $Cu^+(acetone)_x$, $x = 1–4$ clusters are shown in Figure 4 [50].

As pointed out earlier [51], many commonly used aprotic solvents are characterized by a permanent dipole in which the positive charge is diffusely distributed over a large part of the molecule while the negative charge is concentrated in a small, accessible end of the molecule. For acetone, this corresponds to the lone pair of electrons on the carbonyl oxygen atom. Thus it is not surprising that the calculations find that the Cu^+ ion prefers to be bound to the lone pair of electrons on the carbonyl oxygen atom along the axis of the C=O bond, rather than to the π-electrons of the C=O bond. Attempts to calculate a stable Cu^+(acetone) complex in which Cu^+ binds to the π-electrons of the C=O bond always converged to the structure in which binding occurs to the lone pair of electrons on the carbonyl oxygen atom. Thus, calculations of structures involving binding of Cu^+ to the π-electrons of the C=O bond(s) were not pursued for the larger clusters. The distortion of the acetone molecule that occurs upon complexation to Cu^+ is very minor. The change in geometry is largest for the smallest cluster, Cu^+(acetone), and decreases with increasing number of solvent molecules. Bond lengths and bond angles change in the most extreme cases by less than 0.029 Å and 3.2°, respectively. The arrangement of the acetone molecules around the copper ion in the $Cu^+(acetone)_x$ clusters approaches the

Table 4. B3LYP/6-31G* geometry optimized structures of acetone and $Cu^+(acetone)_x$, $x = 1–4$[a]

	Bond length (Å)				Bond angle (°)				
Species	Cu^+–O	C=O	C–C	C–H	OCu^+O	Cu^+OC	CCC	CCH	HCH
acetone	-	1.216	1.521	1.097 (4)	-	-	116.5	110.5 (4)	109.6 (4)
				1.092 (2)				109.9 (2)	106.8 (2)
Cu^+(acetone)	1.734	1.245	1.495	1.098 (4)	-	180.0	119.7	109.7 (4)	109.8 (4)
				1.091 (2)				111.5 (2)	106.2 (2)
$Cu^+(acetone)_2$	1.762	1.240	1.499	1.097 (8)	179.9	179.9	119.3	109.8 (8)	109.7 (8)
				1.091 (4)				111.2 (4)	106.3 (4)
$Cu^+(acetone)_3$	1.881 (2)	1.240 (2)	1.502	1.097 (12)	124.8	158.5	119.2	110.2 (12)	109.6 (12)
	1.903	1.237		1.092 (6)	121.0	134.9		110.5 (6)	106.6 (6)
					114.2	129.2			
$Cu^+(acetone)_4$	1.966	1.237	1.505	1.097 (16)	97.5 (2)	134.0 (2)	118.3	110.8 (16)	109.6 (16)
				1.092 (8)	103.5 (2)	139.8 (2)		109.2 (8)	106.9 (8)
					129.4 (2)				

[a]Average values are provided when there exists more than one essentially equivalent bond length or bond angle. In cases where like atoms are involved but are found to be inequivalent, the numbers in parentheses indicate the number of bond lengths or bond angles that are equivalent. When no numbers are given in parentheses, all bond lengths or angles are equivalent.

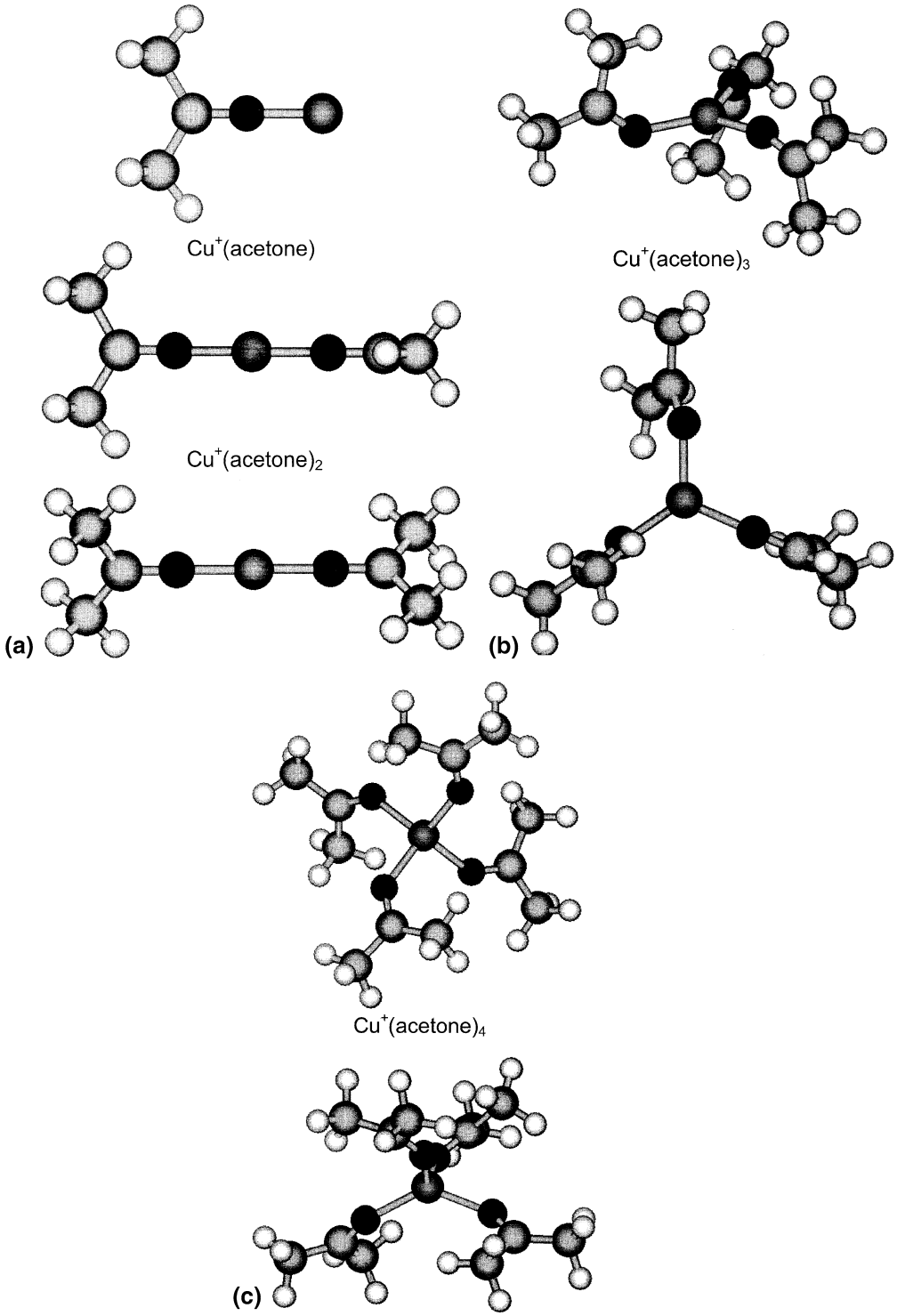

Figure 4. Optimized B3LYP/6-31G* ground state geometries of $Cu^+(acetone)_x$, $x = 1–4$. The $x = 1$ complex and two views of the $x = 2$ complex are shown in part (**a**), two views of the $x = 3$ and 4 complexes are shown in parts (**b**) and (**c**), respectively.

Table 5. Enthalpies and free energies of binding of $Cu^+(acetone)_x$, x = 1–4 at 298 K in kJ/mol[a]

System	ΔH_0	ΔH_0[b]	$\Delta H_{298}-\Delta H_0$[b]	ΔH_{298}	ΔH_{298}[b]	$T\Delta S_{298}$[b]	ΔG_{298}	ΔG_{298}[b]
Cu^+(acetone)	198.6 (4.3)	180.1	3.2 (0.3)	201.8 (4.3)	183.3	24.4 (0.2)	177.4 (4.3)	158.9
$Cu^+(acetone)_2$	209.8 (6.5)	192.9	0.2 (0.5)	210.0 (6.5)	193.1	39.5 (2.8)	170.5 (7.1)	153.6
$Cu^+(acetone)_3$	64.3 (2.4)	54.4	1.3 (2.0)	65.6 (3.1)	55.7	53.3 (3.9)	12.3 (5.0)	2.4
$Cu^+(acetone)_4$	61.0 (5.4)	44.9	0.6 (1.5)	61.6 (5.6)	45.5	46.6 (5.4)	15.0 (7.8)	−1.1

[a]Uncertainties are listed in parentheses.
[b]Ab initio values from calculations at the MP2(full/6-311+G(2d,2p)//B3LYP/6-31G* level of theory.

ideal structures predicted by the valence shell electron pair repulsion (VSEPR) model, e.g., linear for x = 1 and 2, trigonal planar for x = 3, and tetrahedral for x = 4 [52]. However, modest deviations from these idealized structures are observed for the x = 3 and 4 clusters. The Cu^+–O bond lengths increase as the number of acetone molecules surrounding the Cu^+ ion increases. All of the Cu^+–O bond lengths are equivalent for the x = 2, and 4 clusters, but are not equivalent for the x = 3 cluster. In addition, the OCu^+O bond angles are not all equivalent in either structure. It can therefore be assumed that the third and even the fourth acetone molecules do not provide a strong enough ligand field to completely overcome 4s-3d σ hybridization effects of the Cu^+ ion (see discussion below). It is interesting to note that for the x = 1 and 2 clusters, the Cu^+ ion lies along the dipole moment of the acetone ligand, whereas this is not the case for the x = 3 and 4 clusters. These deviations are likely the result of steric effects associated with the crowding of multiple ligands around the copper ion.

Conversion from 0 to 298 K

To allow comparison to commonly used experimental conditions, we convert the 0 K bond energies determined here (experimentally and theoretically) to 298 K bond enthalpies and free energies. The enthalpy and entropy conversions are calculated using standard formulas (assuming harmonic oscillator and rigid rotor models) and the vibrational and rotational constants determined for the B3LYP/6-31G* optimized geometries, which are given in Tables 1 and 2. Table 5 lists 0 and 298 K enthalpy, free energy, and enthalpic and entropic corrections for all systems experimentally determined (from Table 3). Uncertainties in the enthalpic and entropic corrections are determined by 10% variation in the molecular constants. Because theory may not adequately describe the weak interactions in these systems, the listed uncertainties also include contributions from scaling all frequencies below 150 cm^{-1} up and down by a factor of two. The latter provides a conservative estimate of the computational errors in these low frequency modes and is the dominant source of the uncertainties listed.

Discussion

Comparison of Theory and Experiment

The sequential BDEs for the $Cu^+(acetone)_x$, x = 1–4 clusters at 0 K measured here by guided ion beam mass spectrometry are summarized in Table 6. The value for x = 4 represents the value obtained from fitting the total cross section with an error estimate that takes into account the different threshold values obtained fitting both the primary CID channel and the total cross section. Also listed here are the 0 K BDEs calculated at both the B3LYP/6-311+G(2d,2p)//B3LYP/6-31G* and MP2(full)/6-311+G(2d,2p)//B3LYP/6-31G* levels, including zero point energy corrections and basis set

Table 6. Bond dissociation enthalpies of $Cu^+(acetone)_x$, x = 1–4 at 0 K in kJ/mol

		Theory					
	Experiment	B3LYP			MP2		
Complex	TCID[a]	D_e[b]	D_0[b,c]	$D_{0,BSSE}$[b,d]	D_e[e]	D_0[c,e]	$D_{0,BSSE}$[d,e]
Cu^+(acetone)	198.6 (4.3)	206.3	203.0	200.6	195.7	192.4	180.1
$Cu^+(acetone)_2$	209.8 (6.5)	198.6	194.6	191.2	208.9	204.9	192.9
$Cu^+(acetone)_3$	64.3 (2.4)	67.0	62.6	59.9	73.9	69.4	54.4
$Cu^+(acetone)_4$	61.0 (5.4)	39.1	37.2	34.0	65.2	63.4	44.9
MAD[f]			11.3 (10.2)	13.0 (11.9)		4.6 (1.6)	15.3 (3.8)

[a]Present results, threshold collision-induced dissociation.
[b]Calculated at the B3LYP/6-31+G(2d,2p) level of theory using B3LYP/6-31G* optimized geometries.
[c]Including zero point energy corrections with B3LYP/6-31G* frequencies scaled by 0.9804.
[d]Also includes basis set superposition error corrections.
[e]Calculated at the MP2(full)/6-311+G(2d,2p) level of theory using the B3LYP/6-31G* optimized geometries.
[f]Mean Absolute Deviation (MAD) between 0 K experimentally measured (TCID) values and theoretically calculated values.

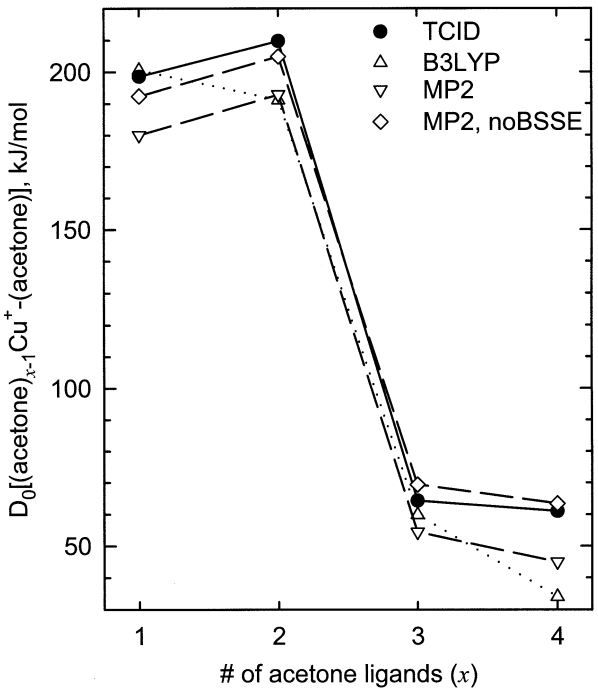

Figure 5. Experimental and theoretical bond energies at 0 K (in kJ/mol) of [(acetone)$_{x-1}$Cu$^+$–acetone] plotted versus x.

superposition error corrections [53, 54]. The agreement between theory and experiment is illustrated in Figure 5.

Cu$^+$(acetone)$_x$, x = 1–2

The present results are the first direct measurements of the BDEs for the Cu$^+$(acetone) and Cu$^+$(acetone)$_2$ complexes. As can be seen in Figure 5, excellent agreement between B3LYP theory and experiment is found for the Cu$^+$(acetone) cluster. The experimental values lie 2.0 kJ/mol below the B3LYP value, well within the experimental error of this measurement (4.3 kJ/mol) and the expected accuracy of this level of theory. The agreement between MP2 theory and experiment is much poorer. The MP2 value is 18.5 kJ/mol lower than the experimental value. It has previously been suggested that BSSE corrections overestimate the effects associated with the differing sizes of the basis set used to calculate the cluster versus the products and can lead to binding energies that are too low [55]. Indeed, much better agreement is obtained when BSSE corrections are not included. In this case, the MP2 value lies 6.2 kJ/mol below the measured value.

The agreement between B3LYP theory and experiment is not nearly so good for the Cu$^+$(acetone)$_2$ cluster. In contrast to the measured value, B3LYP finds a weaker bond for this cluster than the Cu$^+$(acetone) cluster. The B3LYP value lies 18.6 kJ/mol below the value measured here. The MP2 value agrees well with the B3LYP and is 16.9 kJ/mol below the measured value. Again, much better agreement is found when BSSE corrections are not included. In this case, the MP2 value lies 4.9 kJ/mol below the measured value, well within the experimental error of this measurement (6.5 kJ/mol) and the expected accuracy of this level of theory. In contrast to that found using B3LYP theory, MP2 finds a stronger bond for the second ligand regardless of whether or not BSSE corrections are included, consistent with the experimentally measured trend. Similar results have previously been noted in an earlier study of the solvation of Cu$^+$ by CH_3OCH_3, where B3LYP theory failed to accurately predict the relative bond energies of the first two ligands to Cu$^+$, whereas MP2 theory was found to do a much better job [28].

Cu$^+$(acetone)$_x$, x = 3–4

The BDEs for Cu$^+$(acetone)$_x$, x = 3 and 4 have not been previously measured. As can be seen in Figure 5, the theoretical BDEs for these clusters are consistently lower than the experimentally determined values. In fact, the deviation between the calculated and measured values increases with increasing size of the cluster. For the x = 3 cluster, the B3LYP values lies 4.4 kJ/mol below the experimental value, just outside the experimental error of this measurement (2.4 kJ/mol), but well within the expected accuracy of this level of theory. The agreement between MP2 theory and experiment is poorer. The MP2 value is 9.9 kJ/mol lower than the experimental value. Again, much better agreement is observed when BSSE corrections are not included. In this case, the MP2 value lies 5.1 kJ/mol above the experimental value. The agreement between B3LYP theory and experiment is not nearly as good for the x = 4 cluster. The B3LYP value lies 27.0 kJ/mol below the experimental value. The MP2 value is in better agreement with theory but is also lower than the experimental value by 16.1 kJ/mol. Once again, much better agreement is observed when BSSE corrections are not included. In this case, the MP2 value lies 2.4 kJ/mol above the measured value.

Overall, the observed agreement between theory and experiment seems reasonable, Table 6. The mean absolute deviation (MAD) between the experimentally measured and B3LYP values is 13.0 ± 11.9 kJ/mol. Although not a large effect, the MAD for the B3LYP values improves to 11.3 ± 10.2 kJ/mol when BSSE corrections are not included. The MAD for the MP2 values is larger, 15.3 ± 3.8 kJ/mol. As discussed earlier, agreement with the experimental values greatly improves for the MP2 values when BSSE corrections are not included. In this case, the MAD between theory and experiment is only 4.6 ± 1.6 kJ/mol. Thus the current results support the suggestion by Feller that BSSE corrections can lead to binding energies that are too low [55].

Trends in the Sequential BDEs

The BDEs of Cu$^+$(acetone)$_x$ are observed to increase from x = 1 to 2 and both are quite strong. A sharp decrease in the BDE occurs for x = 3, and then a fairly

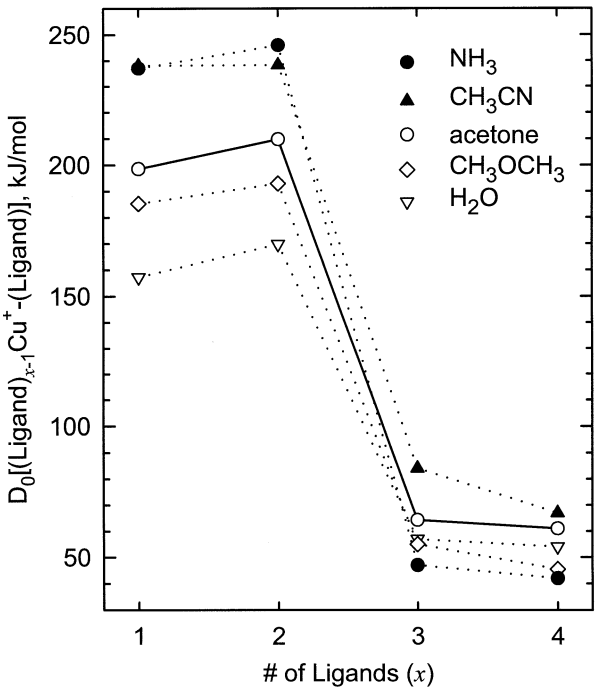

Figure 6. Experimental bond dissociation energies at 0 K (in kJ/mol) of [(ligand)$_{x-1}$Cu$^+$–(ligand)] plotted versus the number of ligands x. Literature values are taken from Vitale et al. for CH_3CN [11], Dalleska et al. for H_2O [26], Walter and Armentrout for NH_3 [27], and Koizumi et al. for CH_3OCH_3 [28].

small decrease is observed for $x = 4$. Similar behavior has been observed in the solvation of Cu^+ binding to several other ligand molecules, e.g., CH_3CN [11], H_2O [25, 26], NH_3 [27], and CH_3OCH_3 [28]. A comparison of the trends in the sequential binding energies of Cu^+ to acetone and the ligands mentioned above is shown in Figure 6. As can be seen in the figure, the trends in the sequential binding energies are very similar for all five ligands. Binding to the nitrogen containing ligands is stronger for the $x = 1$ and 2 clusters. Ammonia appears to be the most strongly bound ligand, but as observed earlier, the sum of the BDEs for the $x = 1$ and 2 ligands appears to be too high by ~28 kJ/mol. The relative errors in the individual BDEs is not known, but comparison to other ligands suggests that the relative values are reasonable and that both BDEs are too high. In this case, CH_3CN would be more strongly bound than NH_3 as expected based upon the dipole moments and polarizabilities of these two ligands, 3.92 and 1.47 D [56] and 4.48 and 2.26 Å^3 [57], respectively. In contrast, NH_3 appears to be the most weakly bound ligand for the $x = 3$ and 4 clusters. For all four other ligands, the trends are very nearly parallel. Amongst the oxygen containing ligands, binding to acetone is stronger than to dimethylether, which in turn is stronger than to water. This trend also parallels the polarizability of these oxygen ligands, 6.40, 5.15, and 1.45 Å^3, respectively. However, this trend differs somewhat from trend in the dipole moments for these ligands, 2.88, 1.30, and 1.85 D, respectively. This suggests that the much larger polarizability of dimethylether compared to water overcomes the smaller dipole moment.

These trends in the sequential BDEs of the $Cu^+(ligand)_x$ clusters can be understood on the basis of two effects that were first explained by Bauschlicher et al., 4s-3d σ hybridization of Cu^+ and ligand–ligand repulsion [58]. They attributed the very strong bonds for the first two solvent molecules to the presence of 4s-3d σ hybridization of the orbitals on Cu^+. Cu^+ is a $4s^03d^{10}$ ion, thus the d σ orbital is occupied and leads to greater Pauli repulsion between the metal ion and the ligand than when it is unoccupied. 4s-3d σ hybridization is one mechanism by which that Pauli repulsion can be reduced by hybridizing electron density away from the ligand in a direction perpendicular to the bonding axis. This allows the first two ligands to approach Cu^+ with minimum electronic repulsion. As can be seen in Figure 6, the BDE to the second ligand is generally stronger than to the first ligand because the energetic cost associated with the hybridization of these orbitals is paid for by the first ligand.

4s-3d σ hybridization effects continue to influence the larger clusters because additional ligands placed around Cu^+ experience greater electron repulsion with the occupied 4s-3d σ orbital. This results in much weaker BDEs for these additional ligands. 4s-3d σ hybridization effects also exert an influence on the geometry of the larger clusters. As mentioned above, the deviations from ideal VSEPR structures found for the $x = 3$ and 4 clusters are likely the result of 4s-3d σ hybridization effects. The third acetone molecule does not appear to provide a strong enough ligand field to overcome these effects such that two of the Cu^+–O bonds are shorter than the third, Table 3, indicating stronger binding to these ligands. In addition, the corresponding OCu^+O bond angle, for the more tightly bound acetone molecules, is closer to linear. Addition of the fourth acetone appears to provide a strong enough ligand field to overcome most of the 4s-3d σ hybridization effects resulting in 4 equivalent Cu^+–O bonds. However, the ligand field created by these four acetone molecules is still not able to completely overcome the 4s-3d σ hybridization effects as the OCu^+O bond angles are not all equivalent. Similar effects associated with the geometries of the $Cu^+(ligand)_x$, $x = 3$ and 4 clusters were also observed for other ligands [11, 28].

Ligand–ligand repulsion also influences the binding energies and geometries of the multiply ligated complexes. The bond energies decrease with increasing ligation as a result of two effects that act in concert. Increasing ligation leads to increasing electrostatic repulsion between the ligands. In addition, the individual electrostatic interactions become weaker because the positive charge on Cu^+ is stabilized by multiple interactions with the lone pairs of electrons from the carbonyl oxygen atoms. Both effects act in concert to increase the distance between Cu^+ and the ligands, resulting in weaker binding.

Table 7. Anchoring of the relative $Cu^+L_2 \rightarrow Cu^+ + 2$ L affinity scale

System	ΔH_0	ΔG_{393}	ΔH_{393}-ΔH_0	$T\Delta S_{393}$	ΔH_0	$\Delta(\Delta H_0)$
$Cu^+(H_2O)$	157.3 (7.7)[a]		3.4 (0.4)[c]	30.2 (2.6)[c]		
$Cu^+(H_2O)_2$	169.8 (6.8)[a]		3.1 (1.0)[c]	48.1 (2.3)[c]		
Sum of BDEs	327.1 (14.5)[a]	226.1 (8.4)[b]	6.5 (1.4)[c]	78.3 (4.9)[c]	297.9 (9.8)	29.2 (17.5)
$Cu^+(CH_3OCH_3)$	185.3 (11.6)[d]		0.3 (1.4)[d]	36.4 (5.4)[d]		
$Cu^+(CH_3OCH_3)_2$	193.0 (7.7)[d]		−3.9 (0.6)[d]	44.9 (8.2)[d]		
Sum of BDEs	378.3 (19.3)[d]	268.2 (8.4)[be]	−3.6 (2.0)[d]	81.3 (13.6)[d]	353.1 (16.1)	25.2 (25.1)
Cu^+(acetone)	198.6 (4.3)[f]		3.9 (0.3)[f]	33.3 (0.3)[f]		
$Cu^+(acetone)_2$	209.8 (6.5)[f]		−0.4 (0.5)[f]	52.0 (3.6)[f]		
Sum of BDEs	408.4 (10.8)[f]	310.5 (8.4)[b]	3.5 (0.8)[f]	85.3 (3.9)[f]	392.3 (9.3)	16.1 (14.2)
$Cu^+(NH_3)$	237.0 (14.0)[g]		6.1 (0.4)[c]	37.7 (0.2)[c]		
$Cu^+(NH_3)_2$	246.0 (9.6)[g]		3.6 (1.3)[c]	52.5 (4.4)[c]		
Sum of BDEs	483.0 (23.6)[g]	346.0 (8.4)[b]	9.7 (1.7)[c]	90.2 (4.6)[c]	426.5 (9.7)	56.5 (25.5)
$Cu^+(CH_3CN)$	238.1 (3.2)[c]		1.8 (1.2)[c]	40.3 (4.1)[c]		
$Cu^+(CH_3CN)_2$	238.3 (8.6)[c]		−1.2 (0.5)[c]	51.5 (5.6)[c]		
Sum of BDEs	476.4 (11.8)[c]	356.9 (8.4)[b]	0.6 (1.7)[c]	91.8 (9.7)[c]	448.1 (12.9)	28.3 (17.5)

[a]Dalleska et al. [26]
[b]Deng and Kabarle [24]
[c]Vitale et al. [11]
[d]Koizuma et al. [28]
[e]Jones and Staley [23]
[f]Present results.
[g]Walter and Armentrout [27]

Anchoring of the Relative $Cu^+L_2 \rightarrow Cu^+ + 2L$ Affinity Scale

In their work on the determination of total bond energies of copper ion–ligand L complexes, CuL_2^+, Jones and Staley reported relative free energies for the reaction, $CuL_2^+ = Cu^+ + 2L$ for some 43 different ligands. These values were determined by measuring exchange equilibria of the type $Cu^+A_2 + 2B \rightleftarrows CuB_2^+ + 2A$ in an ion cyclotron resonance mass spectrometer (ICR MS) [23]. The ligands they examined were relatively weakly bonding ligands, most of which were oxygen bases, and included acetone. In later work, Deng and Kebarle measured further equilibria of this type in a high-pressure mass spectrometer (HPMS) for 23 different ligands [24]. The ligands they examined included 10 of the original ligands examined by Jones and Staley as well as more strongly bonding nitrogen bases. Deng and Kebarle converted the relative values they measured to absolute values by anchoring those values using theoretical values determined by Bauschlicher and co-workers [58] for $Cu^+(NH_3)_2$. Deng and Kebarle chose to anchor their results in this way because the only experimentally measured values available at that time were for $Cu^+(H_2O)_2$ [25], which was not directly measured in their study, but was included in the absolute values they reported. In addition, Deng and Kebarle missed work by Dalleska et al. [26] who had also measured the sequential BDEs of H_2O to the first-row transition-metal monocations by threshold CID techniques. If Dalleska et al.'s measured values for the $Cu^+(H_2O)_x$, $x = 1$–2 complexes are combined and compared to the value reported by Deng and Kebarle, after appropriate temperature corrections [59], a difference of 29.2 ± 17.5 kJ/mol in the total binding energy of $Cu^+(H_2O)_2$ at 0 K is found, Table 7. This suggests that Deng and Kebarle's choice of the theoretical binding energy for $Cu^+(NH_3)_2$, calculated by Bauschlicher and co-workers, to anchor their values leads to absolute values that are too low. Since this time, there have been several additional studies of the sequential BDEs of various ligands to Cu^+, which might also be used to anchor the CuL_2^+ relative affinity scale. The first of these is a study by Walter and Armentrout [27] that appeared at about the same time that Deng and Kebarle's work appeared. In this study, Walter and Armentrout measured the sequential BDEs of NH_3 to the first-row transition-metal monocations by threshold CID techniques. If Walter and Armentrout's measured values for the $Cu^+(NH_3)_x$, $x = 1$–2 complexes are combined and compared to the value reported by Deng and Kebarle, after appropriate temperature corrections [60], a difference of 56.5 ± 25.5 kJ/mol is found, Table 7. This too suggests that all of the values reported by Deng and Kebarle are too low. However, this work suggests that Deng and Kebarle's values should be raised by a much larger amount. Recently, Koizumi et al. [28] measured the sequential BDEs of dimethylether, CH_3OCH_3, to Cu^+, again using threshold CID techniques. If Koizumi et al.'s measured values for the $Cu^+(CH_3OCH_3)_x$, $x = 1$–2 complexes are combined and compared to the values reported by Jones and Staley, and Deng and Kebarle, after appropriate temperature corrections, a difference of 25.2 ± 25.1 kJ/mol is found, Table 7. This too suggests that the values reported by Deng and Kebarle are too low, but by a similar amount to that found when Dalleska et al.'s values for H_2O are used to anchor the scale. Another recent study by Vitale et al. [11], in which the sequential BDEs of CH_3CN to Cu^+ were measured using threshold CID techniques, might also be used to anchor the CuL_2^+ relative affinity scale.

If Vitale et al.'s measured values for the $Cu^+(CH_3CN)_x$, $x = 1–2$ complexes are combined and compared to the value reported by Deng and Kebarle, after appropriate temperature corrections, a difference of 28.3 ± 17.5 kJ/mol is found, Table 7. Yet again, the absolute values measured in this study suggest that the values reported by Deng and Kebarle are too low. Finally, the values measured here for acetone might also be used to anchor the CuL_2^+ relative affinity scale. If the values measured here for $Cu^+(acetone)_x$, $x = 1–2$ complexes are combined and compared to the value reported by Deng and Kebarle, after appropriate temperature corrections, a difference of 16.1 ± 14.2 kJ/mol is found, Table 7. Thus the work performed here also suggests that the values reported by Deng and Kebarle are too low.

From the above analysis, it seems clear that use of Bauschlicher and co-workers theoretical values for $Cu^+(NH_3)_x$ to anchor Deng and Kebarle's scale of Cu^+ binding affinities was inappropriate and results in absolute values that are too low. Additional support for this conclusion comes from the more accurate theoretical calculations performed by Vitale et al. for these clusters. At the B3LYP/6-311+G(2d,2p)//B3LYP/6-31G* level of theory, they calculate a total binding energy for $Cu^+(NH_3)_2$ that is 8.5 kJ/mol greater than that calculated by Bauschlicher and co-workers. Likewise, the use of Walter and Armentrout's values for $Cu^+(NH_3)_x$, $x = 1–2$ complexes to anchor Deng and Kebarle's scale of Cu^+ binding affinities results in absolute values that appear too high compared to the other four studies. However, it should be noted that the used of Walter and Armentrout's values to anchor the CuL_2^+ relative affinity scale still results in values that fall within the combined experimental errors of these measurements. The conclusion that Walter and Armentrout's values might be too high comes from comparison of their values with the theoretical values determined by Vitale et al. The total theoretical binding energy they calculate for $Cu^+(NH_3)_2$ is 33.5 kJ/mol lower than that derived from Walter and Armentrout's measurements. Support for the reliability of Dalleska et al.'s measurements comes from comparison to the theoretical values determined by Vitale et al. The total theoretical binding energy Vitale et al. calculate for $Cu^+(H_2O)_2$ is only 9.2 kJ/mol lower than that derived from Dalleska et al.'s measurements, well within the experimental error of these measurements. Finally, the theoretical total binding energy Vitale et al. calculate for $Cu^+(CH_3CN)_2$ is only 4.5 kJ/mol lower than their measured values, again well within the experimental error of their measurements. Thus internal consistency is achieved for the eight studies involved (Vitale et al., Walter and Armentrout, Jones and Staley, Deng and Kebarle, Magnera et al., Dalleska et al., Koizumi et al., and the present work) when the Cu^+ binding affinities are anchored using the absolute values measured in the any of the threshold CID studies. As mentioned above, the values of Walter and Armentrout appear to be a little too high, but are just within the combined experimental errors of these measurements. This suggests that the absolute values of Cu^+ binding affinities (ΔG°_{393}) reported by Deng and Kebarle should be raised. The results of Dalleska et al. for $Cu^+(H_2O)_x$ suggest that Deng and Kebarle's values should be raised by 29.2 ± 17.5 kJ/mol. The results of Walter and Armentrout for $Cu^+(NH_3)_2$ suggest that Deng and Kebarle's values should be increased by 56.5 ± 25.5 kJ/mol. The results of Vitale et al. for $Cu^+(CH_3CN)_x$ suggest that Deng and Kebarle's values should be increased by 28.3 ± 17.5 kJ/mol. The results of Koizumi et al. suggest that Deng and Kebarle's values should be raised by 25.2 ± 25.1 kJ/mol. The present results suggest that Deng and Kebarle's values need only be raised by 16.1 ± 14.2 kJ/mol. In any case, internal consistency is obtained within the experimental error associated with these measurements. Therefore, the values reported by Dalleska et al. for $Cu^+(H_2O)_x$, Walter and Armentrout for $Cu^+(NH_3)_2$, Vitale et al. for $Cu^+(CH_3CN)_x$, Koizumi et al. for $Cu^+(CH_3OCH_3)_x$, or those reported here for $Cu^+(acetone)_x$ provide accurate absolute values by which relative Cu^+ binding affinities might be anchored. A statistically weighted average of the results from these five studies suggests that Deng and Kebarle's absolute scale should be raised by 27.0 ± 8.3 kJ/mol. The relative values reported by Jones and Staley but not included in Deng and Kebarle's work can also be put on an absolute scale using the results of Koizumi et al. for CH_3OCH_3 or those reported here for acetone; the only two systems they measured in which absolute values have been determined. Using either of these two studies to anchor Jones and Staley's relative values results in values that are consistent to within 5 kJ/mol, well within the experimental error of these measurements.

Conclusions

The kinetic energy dependence of the collision-induced dissociation of $Cu^+(acetone)_x$, $x = 1–4$ with Xe are examined in a guided ion beam mass spectrometer. The dominant dissociation process in all cases is loss of an intact acetone ligand. Thresholds for these processes are determined after consideration of the effects of reactant internal energy, multiple collisions with Xe, and lifetime effects (using methodology described in detail elsewhere) [22]. Insight into the structures and binding energies of the $Cu^+(acetone)_x$ clusters is provided by ab initio and density functional theory calculations of these complexes performed at the B3LYP/6-311+G(2d,2p)//B3LYP/6-31G* and MP2(full)/6-311+G(2d,2p)//B3LYP/6-31G* levels of theory. The present results for all $Cu^+(acetone)_x$ clusters represent the first direct measurement of the BDEs for these complexes. The total binding energy of the $Cu^+(acetone)_2$ complex reported by Deng and Kebarle [24] using measured values by Jones and Staley [23] (once properly anchored) is in very good agreement with the value derived from our measurements. It

should be noted that the values reported by Deng and Kebarle [24] were anchored to theoretical values determined by Bauschlicher and co-workers [58] rather than to experimentally measured values. The values they reported should be correctly anchored to the values measured by Dalleska et al. for H_2O [26], Walter and Armentrout for NH_3 [27], Vitale et al. for CH_3CN [11], Koizumi et al. for CH_3OCH_3 [28], or to the values measured here for acetone. The weighted average of the results from these five studies suggests that Deng and Kebarle's absolute scale should be raised by 27.0 ± 8.3 kJ/mol. The agreement between theory and experiment is reasonable for $x = 1–4$ but varies both with the size of the cluster and the level of theory employed. B3LYP does an excellent job for the $x = 1$ and 3 clusters, but is systematically low for the $x = 2$ and 4 clusters such that the overall trends are not parallel. In contrast, all MP2 values are all somewhat low, but the overall trends parallel the measured values for all clusters. Much better agreement is observed between MP2 theory and experiment when BSSE corrections are not included in support of conclusions made earlier by Feller [55]. The trends in the measured $Cu^+(acetone)_x$ binding energies are explained in terms of sd hybridization effects and ligand–ligand repulsion in the clusters.

Acknowledgments

This work was supported in part by an ASMS Research Award from Micromass.

References

1. Kumpf, R. A.; Dougherty, D. A. A Mechanism for Ion Selectivity in Potassium Channels: Computational Studies of Cation–π Interactions. *Science* **1993,** *261,* 1708–1710.
2. Feller, D.; Dixon, D. A.; Nicholas, J. B. Binding Enthalpies for Alkali Metal Cation–Benzene Complexes Revisited. *J. Phys. Chem. A* **2000,** *104,* 11414–11419.
3. Amicangelo, J. C.; Armentrout, P. B. Absolute Binding Energies of Alkali Metal Cation Complexes with Benzene Determined by Threshold Collision-Induced Dissociation Experiments and ab Initio Theory. *J. Phys. Chem. A* **2000,** *104,* 11420–11432.
4. Izatt, R. M.; Terry, R. E.; Haymore, B. L.; Hansen, N. K.; Dalley, A. G.; Avondet, A. G.; Christensen, J. J. Calorimetric Titration Study of the Interaction of Several Uni- and Bivalent Cations with 15-Crown-5, 18-Crown-6, and Two Isomers of Dicyclohexo-18-Crown-6 in Aqueous Solution at 25 °C and $\mu = 0.1$. *J. Am. Chem. Soc.* **1976,** *98,* 7620–7626.
5. Glendening, E. D.; Feller, D.; Thompson, M. A. An ab Initio Investigation of the Structure and Alkali Metal Cation Selectivity of 18-Crown-6. *J. Am. Chem. Soc.* **1994,** *116,* 10657–10669.
6. Feller, D. Ab Initio Study of M^+:18-Crown-6 Microsolvation. *J. Phys. Chem. A* **1997,** *101,* 2723–2731.
7. More, M. B.; Ray, D.; Armentrout, P. B. Intrinsic Affinities of Alkali Metal Cations for 15-Crown-5 and 18-Crown-6: Bond Dissociation Energies of Gas-Phase M^+–Crown Ether Complexes. *J. Am. Chem. Soc.* **1999,** *121,* 417–423.
8. Armentrout, P. B. Cation–Ether Complexes in the Gas Phase: Thermodynamic Insight into Molecular Recognition. *Int. J. Mass Spectrom.* **1999,** *193,* 227–240.
9. De Jong, F.; Reinhoudt, D. N. Stability and Reactivity of Crown–Ether Complexes. *Adv. Phys. Org. Chem.* **1980,** *17,* 279–433.
10. Valina, A. B.; Amunugama, R.; Huang, H.; Rodgers, M. T. Collision-Induced Dissociation and Theoretical Studies of Na^+–Acetonitrile Complexes. *J. Phys. Chem. A* **2001,** *105,* 11057–11068.
11. Vitale, G.; Valina, A. B.; Huang, H.; Amunugama, R.; Rodgers, M. T. Solvation of Copper Ions by Acetonitrile. Structures and Sequential Binding Energies of $Cu^+(CH_3CN)_x$, $x = 1–5$, from Collision-Induced Dissociation and Theoretical Studies. *J. Phys. Chem. A* **2001,** *105,* 11351–11364.
12. Rodgers, M. T.; Armentrout, P. B. Absolute Alkali Metal Ion Binding Affinities of Several Azoles Determined by Threshold Collision-Induced Dissociation. *Int. J. Mass Spectrom.* **1999,** *185/186/187,* 359–380.
13. Amunugama, R.; Rodgers, M. T. Absolute Alkali Metal Ion Binding Affinities of Several Azines Determined by Threshold Collision-Induced Dissociation and ab Initio Theory. *Int. J. Mass Spectrom.* **2000,** *195/196,* 439–457.
14. Rodgers, M. T.; Stanley, J. R.; Amunugama, R. Periodic Trends in the Binding of Metal Ions to Pyridine Studied by Threshold Collision-Induced Dissociation and Density Functional Theory. *J. Am. Chem. Soc.* **2000,** *122,* 10969–10978.
15. Rodgers, M. T. Substituent Effects in the Binding of Alkali Metal Ions to Pyridines, Studied by Threshold Collision-Induced Dissociation and ab Initio Theory: The Methylpyridines. *J. Phys. Chem. A* **2001,** *105,* 2374–2383.
16. Rodgers, M. T. Substituent Effects in the Binding of Alkali Metal Ions to Pyridines Studied by Threshold Collision-Induced Dissociation and ab Initio Theory: The Aminopyridines. *J. Phys. Chem. A* **2001,** *105,* 8145–8153.
17. Amunugama, R.; Rodgers, M. T. Periodic Trends in the Binding of Metal Ions to Pyrimidine Studied by Threshold Collision-Induced Dissociation and Density Functional Theory. *J. Phys. Chem. A* **2001,** *105,* 9883–9892.
18. Rodgers, M. T.; Armentrout, P. B. Noncovalent Interactions of Nucleic Acid Bases (Uracil, Thymine, and Adenine) with Alkali Metal Ions. Threshold Collision-Induced Dissociation and Theoretical Studies. *J. Am. Chem. Soc.* **2000,** *122,* 8548–8558.
19. Rodgers, M. T.; Armentrout, P. B. Influence of d Orbital Occupation on the Binding of Metal Ions to Adenine. *J. Am. Chem. Soc.* accepted.
20. Rodgers, M. T.; Armentrout, P. B. Collision-Induced Dissociation Measurements on $Li^+(H_2O)_n$, $n = 1–6$: The First Direct Measurement of the Li^+–OH_2 Bond Energy. *J. Phys. Chem. A* **1997,** *101,* 1238–1249.
21. Rodgers, M. T.; Armentrout, P. B. Statistical Modeling of Competitive Threshold Collision-Induced Dissociation. *J. Chem. Phys.* **1998,** *109,* 1787–1800.
22. Rodgers, M. T.; Ervin, K. M.; Armentrout, P. B. Statistical Modeling of Collision-Induced Dissociation Thresholds. *J. Chem. Phys.* **1997,** *106,* 4499–4508.
23. Jones, R. W.; Staley, R. H. Relative Bond Dissociation Energies for Two-Ligand Complexes of Cu^+ with Organic Molecules in the Gas Phase. *J. Am. Chem. Soc.* **1982,** *104,* 2296–2300.
24. Deng, H.; Kebarle, P. Bond Energies of Copper Ion–Ligand L Complexes CuL_2^+ Determined in the Gas Phase by Ion–Ligand Exchange Equilibria Measurements. *J. Am. Chem. Soc.* **1998,** *120,* 2925–2931.
25. Magnera, T. F.; David, D. E.; Stulik, D.; Orth, R. G.; Jonkman, H. T.; Michl, J. Production of Hydrated Metal Ions by Fast Ion or Atom Beam Sputtering. Collision-Induced Dissociation and Successive Hydration Energies of Gaseous Cu^+ with 1–4 Water Molecules. *J. Am. Chem. Soc.* **1989,** *111,* 5036–5043.
26. Dalleska, N. F.; Honma, K.; Sunderlin, L. S.; Armentrout, P. B. Solvation of Transition Metal Ions by Water. Sequential Binding Energies of $M^+(H_2O)_x$ ($x = 1–4$) for M = Ti to Cu

Determined by Collision-Induced Dissociation. *J. Am. Chem. Soc.* **1994,** *116,* 3519–3528.
27. Walter, D.; Armentrout, P. B. Sequential Bond Dissociation Energies of $M^+(NH_3)_x$ (x = 1–4) for M = Ti–Cu. *J. Am. Chem. Soc.* **1998,** *120,* 3176–3187.
28. Koizumi, H.; Zhang, X.-G.; Armentrout, P. B. Collision-Induced Dissociation and Theoretical Studies of Cu^+–Dimethyl Ether Complexes. *J. Phys. Chem. A* **2001,** *105,* 2444–2452.
29. (a) Teloy, E.; Gerlich, D. Integral Cross Sections for Ion-Molecule Reactions I. The Guided Ion Beam Technique. *Chem. Phys.* **1974,** *4,* 417–427. (b) Gerlich, D. *Inhomogeneous RF Fields: A Versatile Tool for the Study of Processes with Slow Ions*. Diplomarbeit, University of Freiburg, Federal Republic of Germany, 1971. (c) Gerlich, D. State-Selected and State-to-State Ion-Molecule Reaction Dynamics, Part I, Experiment. Ng, C.-Y.; Baer, M., Eds. *In Advances in Chemical Physics series, Vol. LXXXII.* Wiley: New York, 1992; p 1.
30. Dalleska, N. F.; Honma, K.; Armentrout, P. B. Stepwise Solvation Enthalpies of Protonated Water Clusters: Collision-Induced Dissociation as an Alternative to Equilibrium Studies. *J. Am. Chem. Soc.* **1993,** *115,* 12125–12131.
31. Aristov, N.; Armentrout, P. B. Collision-Induced Dissociation of Vanadium Monoxide Ion. *J. Phys. Chem.* **1986,** *90,* 5135–5140.
32. Hales, D. A.; Armentrout, P. B. Effect of Internal Excitation on the Collision-Induced Dissociation and Reactivity of Co_2^+. *J. Cluster Sci.* **1990,** *1,* 127–142.
33. Ervin, K. M.; Armentrout, P. B. Translational Energy Dependence of $Ar^+ + XY \rightarrow ArX^+ + Y$ (XY = H_2, D_2, HD) from Thermal to 30 eV c.m. *J. Chem. Phys.* **1985,** *83,* 166–189.
34. Muntean, F.; Armentrout, P. B. Guided Ion Beam Study of Collision-Induced Dissociation Dynamics: Integral and Differential Cross Sections. *J. Chem. Phys.* **2001,** *115,* 1213–1228.
35. (a) Beyer, T. S.; Swinehart, D. F. Number of Multiply-Restricted Partitions [A1]. *Comm. Assoc. Comput. Machines* **1973,** *16,* 379. (b) Stein, S. E.; Rabinovitch, B. S. Accurate Evaluation of Internal Energy Level Sums and Densities Including Anharmonic Oscillators and Hindered Rotors. *J. Chem. Phys.* **1973,** *58,* 2438–2445. (c) On the Use of Exact State Counting Methods in RRKM Rate Calculations. *Chem. Phys. Lett.* **1977,** *49,* 183–188.
36. (a) Pople, J. A.; Schlegel, H. B.; Raghavachari, K.; DeFrees, D. J.; Binkley, J. F.; Frisch, M. J.; Whitesides, R. F.; Hout, R. F.; Hehre, W. J. Molecular Orbital Studies of Vibrational Frequencies. *Int. J. Quant. Chem. Symp.* **1981,** *15,* 269–278. (b) DeFrees, D. J.; McLean, A. D. Molecular Orbital Predictions of the Vibrational Frequencies of Some Molecular Ions. *J. Chem. Phys.* **1985,** *82,* 333–341.
37. Khan, F. A.; Clemmer, D. C.; Schultz, R. H.; Armentrout, P. B. Sequential Bond Energies of $Cr(CO)_x^+$, x = 1–6. *J. Phys. Chem.* **1993,** *97,* 7978–7987.
38. Chesnavich, W. J.; Bowers, M. T. Theory of Translationally Driven Reactions. *J. Phys. Chem.* **1979,** *83,* 900–905.
39. Schultz, R. H.; Crellin, K. C.; Armentrout, P. B. The Sequential Bond Energies of $Fe(CO)_x^+$ (x = 1–5): Systematic Effects on Collision-Induced Dissociation Measurements. *J. Am. Chem. Soc.* **1991,** *113,* 8590–8601.
40. Meyer, F.; Khan, F. A.; Armentrout, P. B. Thermochemistry of Transition Metal Benzene Complexes: Binding Energies of $M(C_6H_6)_x^+$ (x = 1, 2) for M = Ti to Cu. *J. Am. Chem. Soc.* **1995,** *117,* 9740–9748.
41. Dalleska, N. F.; Honma, K.; Armentrout, P. B. Stepwise Solvation Enthalpies of Protonated Water Clusters: Collision-Induced Dissociation as an Alternative to Equilibrium Studies. *J. Am. Chem. Soc.* **1993,** *115,* 12125–12131.
42. Armentrout, P. B.; Simons, J. Understanding Heterolytic Bond Cleavage. *J. Am. Chem. Soc.* **1992,** *114,* 8627–8633.
43. Frisch, M. J.; Trucks, G. W.; Schlegel, H. B.; Scuseria, G. E.; Robb, M. A.; Cheeseman, J. R.; Zakrzewski, V. G.; Montgomery, J. A., Jr.; Stratmann, R. E.; Burant, J. C.; Dapprich, S.; Millam, J. M.; Daniels, A. D.; Kudin, K. N.; Strain, M. C.; Farkas, O.; Tomasi, J.; Barone, V.; Cossi, M.; Cammi, R.; Mennucci, B.; Pomelli, C.; Adamo, C.; Clifford, S.; Ochterski, J.; Petersson, G. A.; Ayala, P. Y.; Cui, Q.; Morokuma, K.; Malick, D. K.; Rabuck, A. D.; Raghavachari, K.; Foresman, J. B.; Cioslowski, J.; Ortiz, J. V.; Stefanov, B. B.; Liu, G.; Liashenko, A.; Piskorz, P.; Komaromi, I.; Gomperts, R.; Martin, R. L.; Fox, D. J.; Keith, T.; Al-Laham, M. A.; Peng, C. Y.; Nanayakkara, A.; Gonzalez, C.; Challacombe, M.; Gill, P. M. W.; Johnson, B.; Chen, W.; Wong, M. W.; Andres, J. L.; Head-Gordon, M.; Replogle, E. S.; Pople, J. A. *Gaussian 98, Revision A.9.* Gaussian, Inc: Pittsburgh PA, 1998.
44. Becke, A. D. Density-Functional Thermochemistry. III. The Role of Exact Exchange. *J. Chem. Phys.* **1993,** *98,* 5648–5652.
45. Lee, C.; Yang, W.; Parr, R. G. Development of the Colle-Salvetti Correlation-Energy Formula into a Function of the Electron Density. *Phys. Rev. B* **1988,** *37,* 785–789.
46. Foresman, J. B.; Frisch, Æ. *Exploring Chemistry with Electronic Structure Methods; 2nd ed.* Gaussian: Pittsburgh, 1996 p 64.
47. Boys, S. F.; Bernardi, R. The Calculation of Small Molecular Interactions by the Differences of Separate Total Energies. Some Procedures with Reduced Errors. *Mol. Phys.* **1979,** *19,* 553–566.
48. Van Duijneveldt, F. B.; van Duijneveldt-van de Rijdt, J. G. C. M.; van Lenthe, J. H. State of the Art in Counterpoise Theory. *Chem. Rev.* **1994,** *94,* 1873–1885.
49. Lifshitz, C. Recent Developments in Applications of RRKM-QET. *Adv. Mass Spectrom.* **1989,** *11,* 113–729.
50. Figures were generated using the output of Gaussian 98 geometry optimizations in Hyperchem computational chemistry software package, version 5.0, Hypercube Inc., 1997.
51. Davidson, W. R.; Kebarle, P. Ionic Solvation by Aprotic Solvents. Gas Phase Solvation of the Alkali Metal Ions by Acetonitrile. *J. Am. Chem. Soc.* **1976,** *98,* 6125–6133.
52. McKenna, A. G.; McKenna, J. F. Teaching VSEPR Theory. *J. Chem. Edu.* **1984,** *61,* 771–773.
53. Bartlett, R. J. Many-Body Perturbation Theory and Coupled Cluster Theory for Electron Correlation in Molecules. *Annu. Rev. Phys. Chem.* **1981,** *32,* 359–401.
54. Hehre, W. J.; Radom, L.; Schleyer, P. v. R.; Pople, J. A. *Ab Initio Molecular Orbital Theory.* Wiley: New York, 1986.
55. Feller, D. A Complete Basis Set Estimate of Cation–π Bond Strengths: Na^+(ethylene) and Na^+(benzene). *Chem. Phys. Lett.* **2000,** *322,* 543–548.
56. Weast, R. C.; Astle, M. J. *Handbook of Chemistry and Physics.* CRC Press, Inc: Florida, 1982 p 3–61.
57. Miller, K. J. Additivity Methods in Molecular Polarizability. *J. Am. Chem. Soc.* **1990,** *112,* 8533–8542.
58. (a) Bauschlicher, C. W.; Langhoff, S. R.; Partridge, H. The Binding Energies of Cu^+–$(H_2O)_n$ and Cu^+–$(NH_3)_n$ (n = 1–4). *J. Chem. Phys.* **1991,** *94,* 2068–2072. (b) Bauschlicher, C. W.; Partridge, H.; Langhoff, S. R. Theoretical Study of Transition-Metal Ions Bound to Benzene. *J. Phys. Chem.* **1992,** *96,* 3273–3278. (c) Langhoff, S. R.; Bauschlicher, C. W.; Partridge, H.; Sodupe, M. Theoretical Study of One and Two Ammonia Molecules Bound to the First-Row Transition Metal Ions. *J. Phys. Chem.* **1991,** *95,* 10677–10681.
59. Thermal corrections to the values reported by Dalleska et al. [26] were determined by Vitale et al. [11] from theoretical calculations at the B3LYP/6-311 + G(2d,2p)//B3LYP/6-31G* level of theory for H_2O, $Cu^+(H_2O)$, and $Cu^+(H_2O)_2$.
60. Thermal corrections to the values reported by Walter and Armentrout [27] were determined by Vitale et al. [11] from theoretical calculations at the B3LYP/6-311 + G(2d,2p)//B3LYP/6-31G* level of theory for NH_3, $Cu^+(NH_3)$, and $Cu^+(NH_3)_2$.